Airfoil Design and Rotorcraft Performance

WILLIAM G. BOUSMAN

wbousman@mail.arc.nasa.gov
Army/NASA Rotorcraft Division
Aeroflightdynamics Directorate (AMRDEC)
US Army Aviation and Missile Command
Ames Research Center, Moffett Field, California

Abstract

The relationship between global performance of a typical helicopter and the airfoil environment, as represented by the airfoil angles of attack and Mach number, has been examined using the comprehensive analysis CAMRAD II. A general correspondence is observed between global performance parameters, such as rotor *L/D*, and airfoil performance parameters, such as airfoil *L/D*, the drag bucket boundaries, and the divergence Mach number. Effects of design parameters such as blade twist and rotor speed variation have been examined and, in most cases, improvements observed in global performance are also observed in terms of airfoil performance. The relations observed between global performance and the airfoil environment suggests that the emphasis in airfoil design should be for good *L/D*, while the maximum lift coefficient performance is less important.

Introduction

Commercial fixed-wing aircraft are designed to obtain economical performance at their cruise speed. This requires that the wing's airfoil sections be designed to operate at angles of attack that provide the best *L/D* over the aircraft's operational Mach numbers. As fuel is burned off during cruise, angle of attack, altitude, and Mach number are optimized within the constraints of air traffic management requirements. If angle of attack is plotted as a function of Mach number, the loci of all cruise conditions are very close to best *L/D* for the airfoil sections. However, the range of variation in angle of attack is of the order of a degree or two, and the Mach number varies by less than 0.1.

In contrast to the fixed-wing case, the angle of attack and Mach number for a helicopter blade airfoil section at the helicopter's best cruise speed exhibits a wide variation in Mach number and angle of attack. The airfoil sections at the blade tip of a typical helicopter operating at μ = 0.33 will operate at low angles of attack, with Mach numbers over 0.80 on the advancing side, while angles of attack between five and 10 deg, and Mach numbers less than 0.40 will occur on the retreating side.

There is general agreement within the aerodynamic design community that airfoil performance is best optimized by obtaining a balance between the advancing and retreating sides (Refs. 1–3, for example). On the advancing side, airfoils are designed to delay drag divergence to higher Mach numbers, while on the retreating side airfoils are sought that have the greatest maximum lift coefficient. Generally, divergence Mach number, M_{dd}, is evaluated at zero lift, while the maximum lift coefficient, $C_{l_{max}}$, is evaluated at a Mach number of 0.4. These two objectives result in design conflicts for new airfoils, as improvements in divergence Mach number require thin airfoils with limited camber while improved $C_{l_{max}}$ requires thicker airfoils with greater camber. To some degree this conflict is resolved by using thinner airfoils near the tip, to meet the advancing side criteria, and thicker, cambered airfoils inboard that can meet the retreating side criteria. This approach to airfoil design appears to have generally been successful, providing the efficient helicopters that are in operation today.

Nonetheless, the question remains: how efficient are current airfoil sections? The present paper will examine the relationships between the airfoil design environment and helicopter performance using the CAMRAD II analysis (Refs. 4, 5). Example calculations will be made

Presented at the American Helicopter Society 58th Annual Forum, Montréal, Canada, June 11-13, 2002.

for a utility class helicopter similar to the U.S. Army's UH–60A Black Hawk. The paper will start by examining the operating environment of typical helicopter blade sections and make some inferences concerning what features are most important. The examination of the section characteristics will be followed by a discussion of the CAMRAD II model of the UH–60A and global measures of performance. The CAMRAD II analysis will be used to compute both the airfoil section operating environment and helicopter performance over a wide range of operating conditions. The influence of parametric changes in blade twist and rotor speed will be examined. Conclusions will be provided concerning the relationships between the airfoil design environment and helicopter performance.

Airfoil Design Environment

The UH–60A helicopter has a four-bladed rotor which uses two airfoil sections. The SC1095 section extends from the root cutout to 0.48R and also from 0.84R to the blade tip. The SC1094 R8 airfoil covers the midsection of the blade from 0.48R to 0.84R. Outboard of 0.92R the blade is swept aft by 20 deg.

The airfoil design environment is illustrated in Fig. 1, based on wind tunnel measurements of the SC1095 airfoil (Ref. 6). The figure shows the measured L/D as a function of the angle of attack and Mach number. In the Mach number direction, data were obtained from M = 0.34 to 0.87 in increments of 0.05. Along the angle of attack axis, the data were obtained from –4 to 14 deg in increments of 2 deg and smooth curves have been interpolated through the angle of attack data. These measurements are particularly useful because of the fine grid on which the data have been obtained. As observed in the figure, the airfoil L/D is highest at low Mach numbers, varying between 80 and 90 for $M < 0.45$. At these lower Mach numbers the L/D curve is quite broad and the angle of attack at which a maximum in L/D occurs, ranges from 6 to 8 deg. As the Mach number increases, the L/D drops and the angle of attack for maximum L/D becomes progressively lower as well. This angle of attack for maximum L/D, referred to here as $\alpha_{L/D}$, is illustrated in the figure with a thickened, solid line. The maximum lift coefficient, $C_{l_{max}}$, occurs at higher angles of attack and this is shown on the figure with a thickened, dashed line. Note that $C_{l_{max}}$ is undefined for Mach numbers beyond 0.54.

As the rotor blade makes one revolution, from zero to 360 deg, the angle of attack and Mach number at each radial location will define a loop that falls on the surface shown in Fig. 1. If the loop is located to the left of the line for $\alpha_{L/D}$, the lift-to-drag ratio will be less than the maximum, but there will be no penalty in drag, as the airfoil will be operating completely within the drag bucket. If the loop is coincident with the $\alpha_{L/D}$ locus, then the airfoil performance can be considered optimal. If a portion of the loop is above $\alpha_{L/D}$ then there will be a drag penalty for that portion of the loop. Eventually, as blade loading increases, the loop will tend to extend further onto the right hand surface of Fig. 1, until portions of the loop exceed the $C_{l_{max}}$ boundary and excessive drag penalties are incurred in stall.

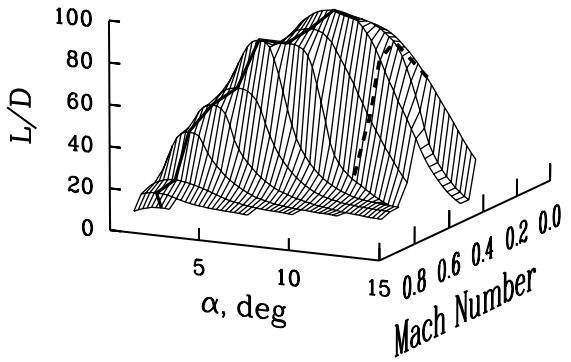

Figure 1. – L/D measured on an SC1095 airfoil shown as a function of angle of attack and Mach number (Ref. 6). Angle of attack for maximum L/D shown as thickened, solid line. Angle of attack for $C_{l_{max}}$ shown as a thickened, dashed line.

Analytical Model

The analytical model used to investigate the relationships between the airfoil section characteristics and global measures of helicopter performance is CAMRAD II (Refs. 4, 5). This model has recently been correlated with UH–60A performance data and has shown generally good results (Ref. 7). The correlation of analysis and measurement was assessed quantitatively and, for the UH–60A, agreement between calculated and measured power was within ±5% for values of the weight coefficient over solidity, C_W/σ, from 0.08 to 0.12. Power was underpredicted at higher weight coefficients, probably because of limitations of the stall modeling used.

The CAMRAD II model from Ref. 7 has been used here with only minor modifications. The aircraft is treated as having single main and tail rotors. The main rotor is modeled as a flexible blade with finite elements. The tail rotor is modeled as an articulated rotor with rigid blades. To simplify parametric calculations, the nonlinear twist of the UH–60A rotor used in Ref. 7 is here replaced

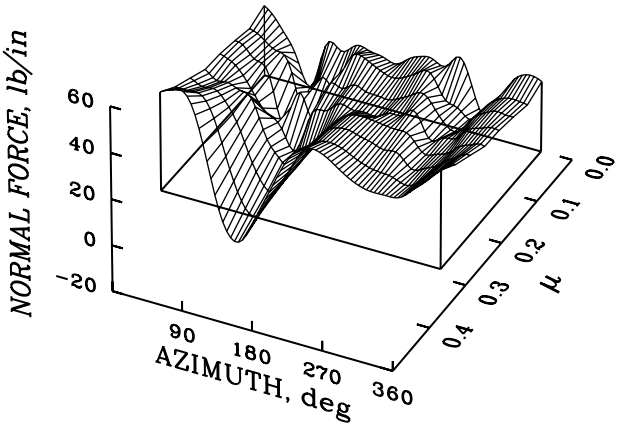

a. CAMRAD II

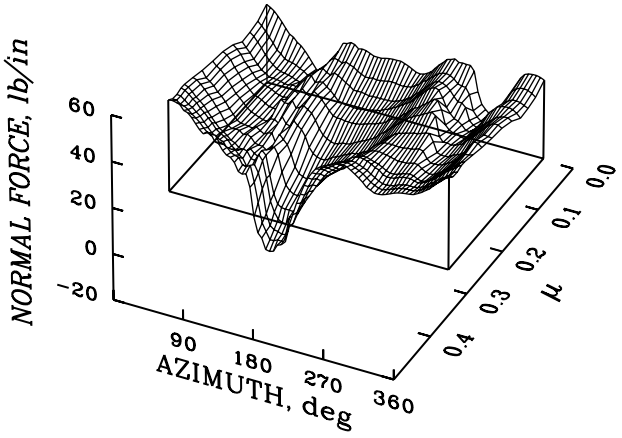

b. UH–60A Airloads Program, Flight 85.

Figure 2. – Comparison of CAMRAD II and flight test measurements for normal force as a function of azimuth and advance ratio; r/R = 0.865. Flight test data from Ref. 8.

with –16 deg of linear twist. The solution is obtained for free-flight trim. The nominal case, $C_W/\sigma = 0.08$, is based on Flight 85 of the NASA/U.S. Army Airloads Program (Ref. 8). Thus, the rotor speed, density, outside air temperature, and the stabilator angle variation with airspeed are assumed to be the same as were measured on Flight 85. The main rotor aerodynamic forces are calculated at the same 18 radial locations as used in Ref. 7. The dual peak free wake model was used for all calculations, but a dynamic stall model was not included. The solution was computed at 15 deg azimuthal intervals.

Figure 2 compares the normal force at 0.865R calculated by CAMRAD II with the flight measurements from Flight 85 of the Airloads Program. The figure shows the normal force as a function of both blade azimuth and advance ratio. For this comparison the advance ratio varies from about 0.09 to 0.37. At low speed, for $\mu \sim 0.1$, rapid variation in normal force is observed on both the advancing and retreating sides and this is a consequence of loading by the disk vortices near the tip of the blade (Ref. 9). As airspeed increases, the disk vortices have less influence on the loading. At high speed, the normal force is dominated by negative loading in the second quadrant and this is typical of a number of helicopters (Ref. 9). Although the CAMRAD II analysis shows good qualitative agreement with the flight data there are a number of quantitative disagreements. In particular, the analysis predicts that the negative loading at high speed occurs about 35 deg earlier than the measurements. This discrepancy appears to be characteristic of most current analyses and there is no acceptable explanation at the present time (Refs. 10, 11).

The good qualitative agreement that is seen here indicates that the CAMRAD II analysis may be used to examine the relationships between the airfoil environment and global performance. However, it will be necessary in examining these relationships to be aware of quantitative limitations of the analysis.

Airfoil and Aircraft Performance

A set of baseline calculations was made for C_W/σ = 0.08 (GW = 16,857 lb) with the advance ratio varying from 0.09 to 0.37 in 0.04 increments. For each advance ratio the angle of attack and Mach number were computed at 18 radial stations and 24 azimuths, giving a total of 432 individual α–M conditions. Multiplied by the eight steps in advance ratio, this provides a total of 3,456 α–M points. These 3,456 points are equally divided between the SC1095 and SC1094 R8 airfoil sections. These points are plotted in Fig. 3 as a function of effective angle of attack, α_{eff}, and effective Mach number, M_{eff}, for both airfoils. The effective angle of attack and Mach number include corrections for sweep and yawed flow effects, and are the values used to enter CAMRAD's two-dimensional airfoil tables in determining the lift, drag, and pitching moment coefficients. Figure 3 also includes indicators that define either the airfoil performance or limitations. Of these, the most important is the angle of attack, $\alpha_{L/D}$, that corresponds to the maximum airfoil L/D. The $\alpha_{L/D}$ characteristic is indicated by a thickened, solid line and has been computed from the airfoil tables used by the CAMRAD II analysis. The thickened, dotted line in the figure shows the upper and lower boundaries of the drag bucket. These boundaries are defined from the airfoil table drag characteristics as shown in Fig. 4. The edges of the drag bucket are identified by looking for a rapid

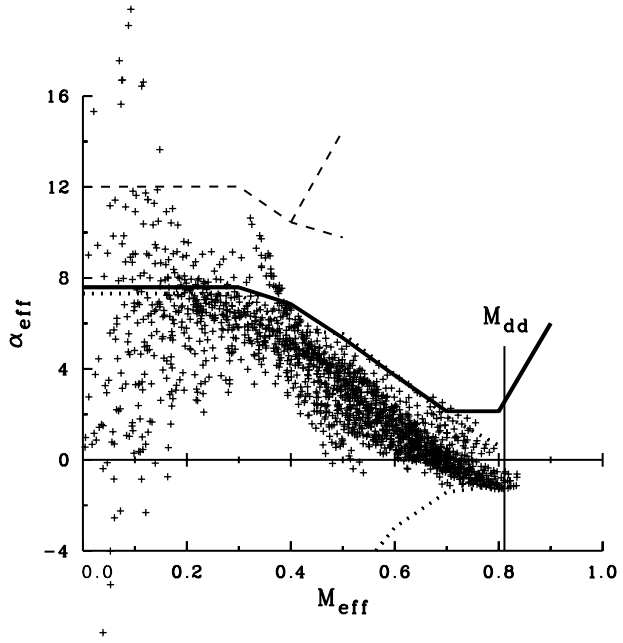

a. SC1095 airfoil section.

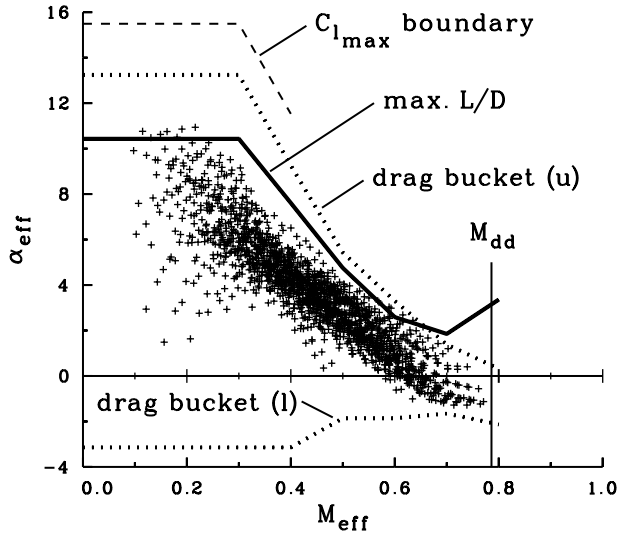

b. SC1094 R8 airfoil section.

Figure 3. – Calculated α_{eff}–M_{eff} points for eight airspeeds for $C_W/\sigma = 0.08$ compared to SC1095 and SC1094 R8 airfoil characteristics.

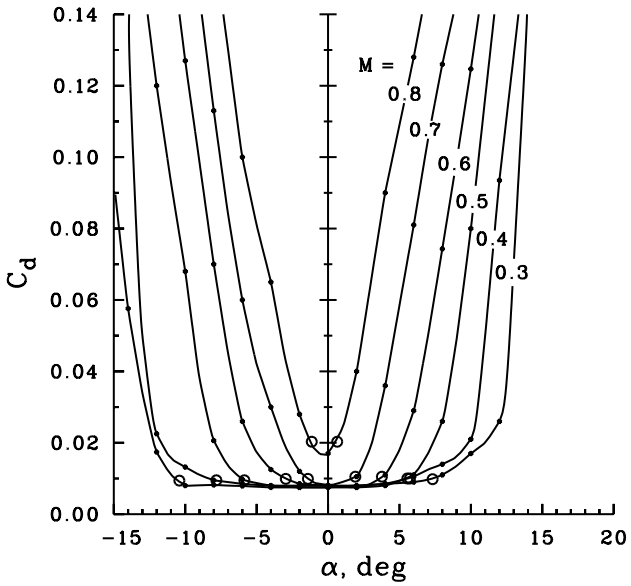

a. SC1095 airfoil section.

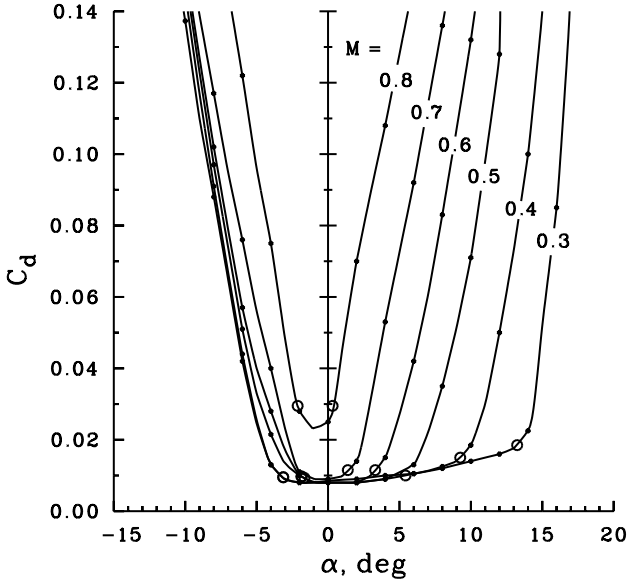

b. SC1094 R8 airfoil section.

Figure 4. – Drag coefficient as a function of angle of attack for SC1095 and SC1094 R8 airfoils; CAMRAD II airfoil tables.

change in slope of the drag coefficient with angle of attack. This is fairly straightforward for the SC1095 airfoil, as the drag bucket is quite flat. However, for the SC1094 R8 airfoil there is some arbitrariness to this procedure as the base of the drag bucket has a slight slope. Thus, at $M = 0.30$, the drag coefficient at the upper or positive boundary is twice as large as the coefficient at the lower or negative boundary. Also shown on Fig. 3, with a dashed line, is the $C_{l_{max}}$ boundary, again calculated from the CAMRAD II airfoil tables. The $C_{l_{max}}$ boundary is not defined above a Mach number of 0.4 or 0.5 as the lift coefficient no longer

shows a maximum at the higher Mach numbers. Note that in the case of the SC1095 airfoil, the tables show two maxima and these are indicated by the bifurcation in the boundary. The last boundary on Fig. 3 is the divergence Mach number, shown by a vertical line.

The α_{eff}–M_{eff} points for the SC1094 R8 are generally lower than the $\alpha_{L/D}$ line and lie within the boundaries of the drag bucket. Thus, for this moderate weight coefficient, the midsection SC1094 R8 airfoil is working mostly below its best *L/D*. The SC1095 airfoil, which is employed both inboard and over the outer 16% of the blade, shows a number of α_{eff}–M_{eff} points that exceed the $\alpha_{L/D}$ line or are outside the drag bucket boundaries. Many of these points occur near the reversed flow boundary and the Mach numbers are so low that the forces on the blade are of no consequence. However, other α_{eff}–M_{eff} pairs exceed these boundaries at higher Mach numbers where the loads are important, most noticeably between a Mach number of 0.3 and 0.4, where an outer blade section α_{eff}–M_{eff} loop is well past the $\alpha_{L/D}$ line and nearly to the $C_{l_{max}}$ boundary.

Effects of Gross Weight

An increase in gross weight translates directly into an increase in blade loading and it is expected that this increase, at some point, will cause degradation in both airfoil and helicopter performance. In this sense, then, the variation in gross weight provides a means of moving from design conditions, where both airfoil and helicopter are near their optimal performance, to off-design conditions where performance is degraded.

The effects of gross weight on helicopter performance are shown in Fig. 5 in terms of rotor *L/D* as a function of airspeed. Best rotor *L/D* occurs between130 and 140 kts (μ = 0.30 to 0.33) and rotor performance is nearly identical for C_W/σ values of 0.08 and 0.09. As the gross weight is further increased, however, there is a noticeable degradation in rotor performance and the advance ratio for best *L/D* occurs at lower airspeeds.

One approach to assessing airfoil performance in these circumstances is to look at the difference between the local angle of attack, α_{eff}, and the angle of attack for maximum *L/D*, $\alpha_{L/D}$. This difference is referred to here as "*L/D* deficiency angle"

$$\alpha_d(r,\psi) = \alpha_{eff}(r,\psi) - \alpha_{L/D}(M)$$

If this difference is zero, then the airfoil performance can be described as optimal. If the *L/D* deficiency angle is negative, the airfoil is not achieving its best performance, but it is also not burdened with a drag penalty. However,

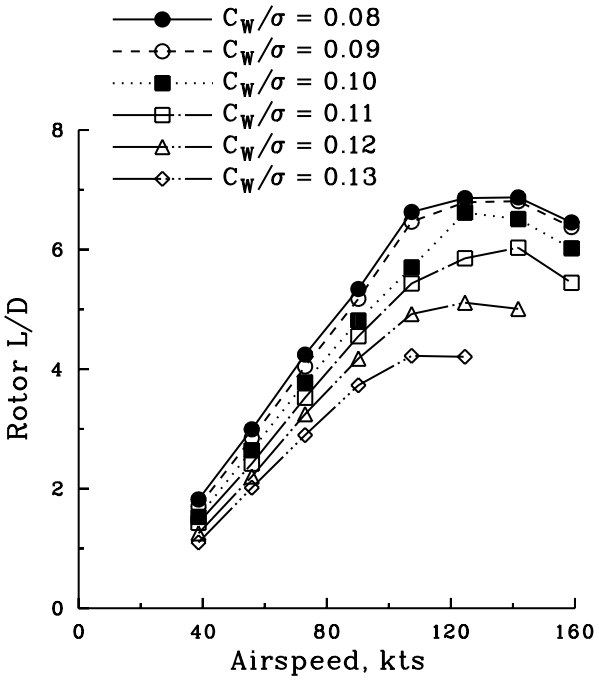

Figure 5. – Rotor *L/D* as a function of airspeed for six weight coefficients; baseline case.

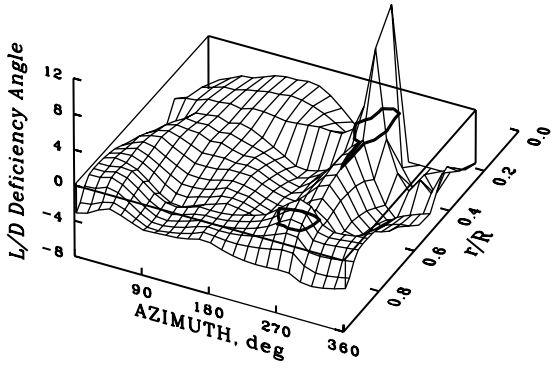

Figure 6. – *L/D* deficiency angle as a function of azimuth and radial station; μ = 0.33, C_W/σ = 0.08. Deficiency angle intersection with zero plane shown with thickened line.

if the deficiency angle is positive, the airfoil may be operating outside of the drag bucket and in that case there is a drag penalty.

The *L/D* deficiency angle is a function of both the radial and azimuthal coordinates. This angle is shown in Fig. 6 for C_W/σ = 0.08 and μ = 0.33 (142 kts). The zero plane of the *L/D* deficiency angle is shown in this figure

and represents the optimal solution for the airfoil. For this fight condition the deficiency angle is negative over most of the r–ψ space. Inboard on the blade the deficiency angle shows both large positive and negative values and although these represent poor performance for the airfoil, the Mach numbers tend to be quite low for these conditions and the forces are minor. Beyond 0.50R the L/D deficiency angle surface is smoother and, for this weight coefficient, is generally negative. On the retreating side there is ridge in the surface where the airfoil is starting to incur a drag penalty and, outboard on the blade, there is a small area where the L/D deficiency angle is positive and the airfoil is starting to exceed the edges of the drag bucket.

One approach to quantifying airfoil performance is to find a simplified method of representing the L/D deficiency angle over the r–ψ space. The mean value of the deficiency angle can be calculated, and variation of this mean with airspeed and gross weight may be examined. This approach is shown in Fig. 7 where the mean L/D deficiency angle is plotted as a function of airspeed for six values of the weight coefficient. There is a general monotonic change in the mean deficiency angle from roughly –2.5 deg at $C_W/\sigma = 0.08$ to between 0 and 1.5 deg at $C_W/\sigma = 0.13$. The rotor L/D shown in Fig. 5 indicates that global performance begins to degrade between $C_W/\sigma = 0.09$ and 0.10. This result appears to conflict with the mean deficiency angle for $C_W/\sigma = 0.10$, shown in Fig. 7, which is less than zero. This difference is because the mean value does not properly represent the variance in the deficiency angle in the r–ψ space. This is illustrated in Fig. 8 where two different approaches are used to quantify the variance in the L/D deficiency angle. The first approach is to calculate the number of α_{eff} –M_{eff} cases where $\alpha_{eff} > \alpha_{L/D}$ and divide by the total number of cases for the flight condition. All cases where $M < 0.10$ are excluded from this ratio. This ratio, referred to as the "L/D angle exceedance," is shown in Fig. 8a. For the moderate lift conditions of $C_W/\sigma = 0.08$ and 0.09, this exceedance is below 10% for most flight conditions. For $C_W/\sigma = 0.10$, the L/D angle exceedance increases to 20–25%, indicating that the airfoil is incurring a drag penalty. (An exceedance angle based on the drag bucket boundary shows the same result.) A second approach is to compute a similar exceedance ratio that is based on the angle of attack exceeding the $C_{l_{max}}$ or stall boundary. This "stall boundary exceedance," is shown in Fig. 8b. This ratio shows a minor hump around 80 kts, which is a result of stall inboard on the blade ($M > 0.10$). Outboard on the blade there is no stall for $C_W/\sigma = 0.08$ and 0.09, but stall becomes increasingly more important as the weight coefficient is increased. Although the stall boundary exceedance ratio is much less than the L/D

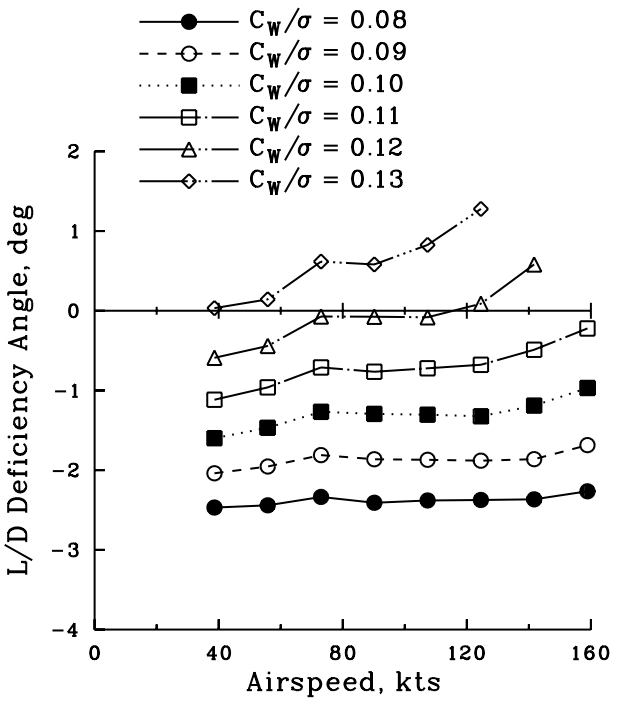

Figure 7. – Mean of L/D deficiency angle as a function of airspeed and weight coefficient. Points with $M < 0.10$ are excluded.

angle exceedance ratio, the drag penalties associated with the former are greater.

A second approach to better understanding the distribution of the L/D deficiency angle in r–ψ space is to calculate the azimuthal mean at each radial station. This approach is shown in Fig. 9, where the azimuthal mean of the L/D deficiency angle is shown as a function of radial station for five weight coefficients at $\mu = 0.33$ (142 kts). At the lowest weight coefficient, the deficiency angle ranges from about –4 to –1 deg along the blade. The distribution of airfoil sections on the blade is evident as there is a break in the deficiency angle at 0.48R and 0.84R. Outboard, the $\alpha_{L/D}$ line is similar for both airfoils and the break is because of differences in angle of attack—the mean chordline of the SC1094 R8 airfoil is offset by –1 deg from the SC1095. Inboard the angles of attack are similar, but $\alpha_{L/D}$ is greater for the SC1094 R8 at these lower Mach numbers. As weight coefficient is increased , the azimuthal mean of L/D deficiency angle is closer to zero with the closest value occurring at about 0.865R. At $C_W/\sigma = 0.10$ the azimuthal mean of the deficiency angle is greater than zero, indicating that the section is near stall or is stalled. The oscillations in the deficiency angle for $C_W/\sigma > 0.10$ are an indication of significant stall on the blade sections, however, some of

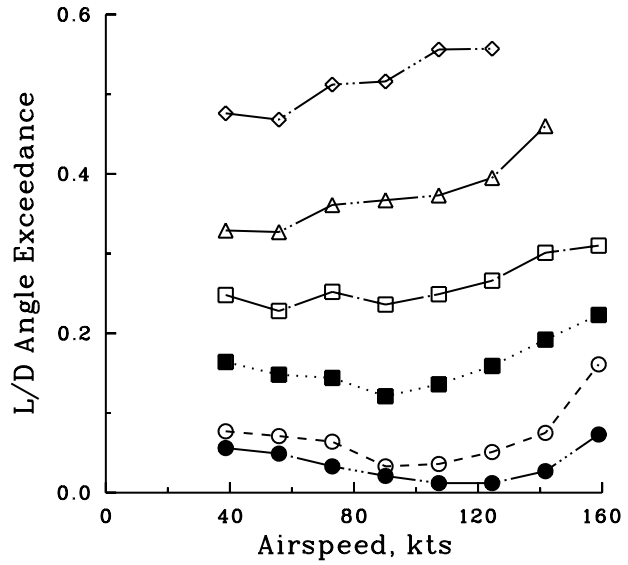

a. *L/D* angle exceedance.

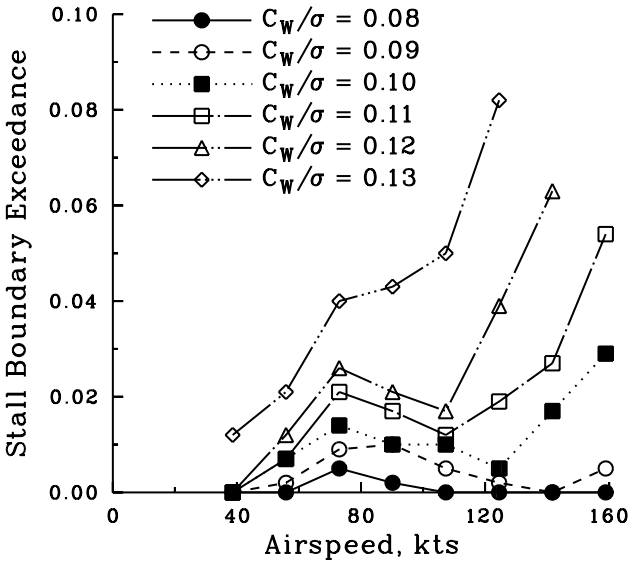

b. Stall boundary exceedance.

Figure 8. – Best *L/D* angle exceedance and stall boundary exceedance as a functions of airspeed and weight coefficient. Points with $M < 0.10$ are excluded.

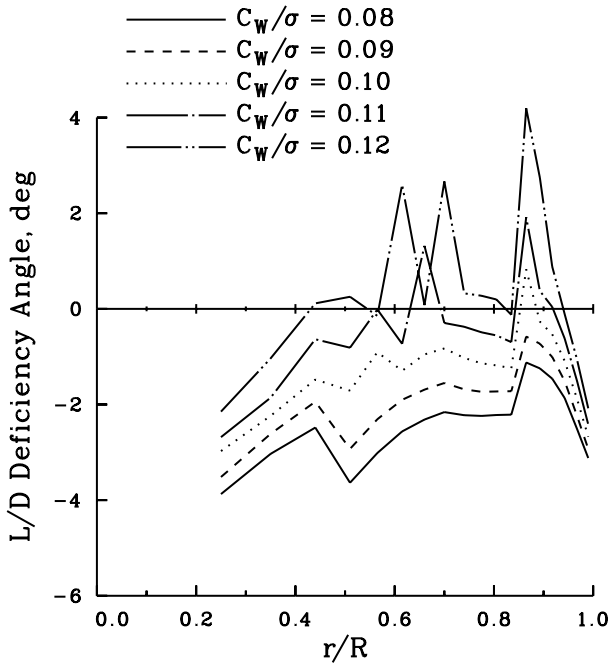

Figure 9. – Azimuthal mean of the *L/D* deficiency angle as a function of radial station for six weight coefficients; $\mu = 0.33$.

this variation is caused by interaction between the CAMRAD II wake and blade section stall.

The radial distribution of the azimuthal mean of the *L/D* deficiency angle appears useful in that it points to radial sections that may be most critical in terms of airfoil performance. Particularly interesting for these baseline calculations are the airfoil sections on either side of the outer transition between the SC1094 R8 and SC1095 airfoils. The $\alpha_{eff} - M_{eff}$ loops at these two locations are shown in Fig. 10 for three values of weight coefficient. Inboard, on the SC1094 R8, the loops generally lie just below the $\alpha_{L/D}$ line. Only the $C_W/\sigma = 0.10$ case exceeds the best *L/D* line, and then only for a limited azimuthal extent. At $0.865R$, on the SC1095, the loops for $C_W/\sigma = 0.08$ and 0.09 lie beneath the $\alpha_{L/D}$ line except for a small bit on the retreating blade where both exceed the best *L/D* boundary. The loop for the $C_W/\sigma = 0.10$ case, however, exceeds the $\alpha_{L/D}$ line over a significant portion of the disk and also exceeds the stall boundary near 270 deg. Although this excursion occurs quickly, it is associated with a large drag increase and hence a performance penalty.

Effects of Blade Twist

Performance calculations shown for the baseline cases in Fig. 5 indicate that degradation in performance caused by blade loading becomes significant between $C_W/\sigma = 0.09$ and 0.10. The previous examination of the airfoil performance for these conditions suggests that this degradation is related to excessive drag and stall outboard

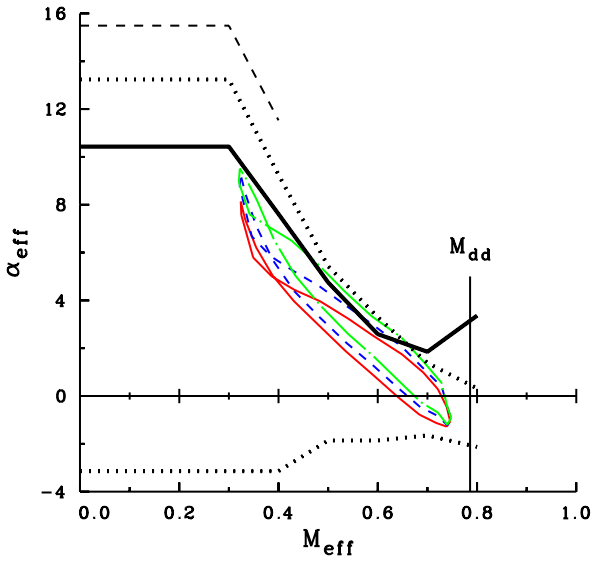

a. 0.835*R* (SC1094 R8 airfoil section).

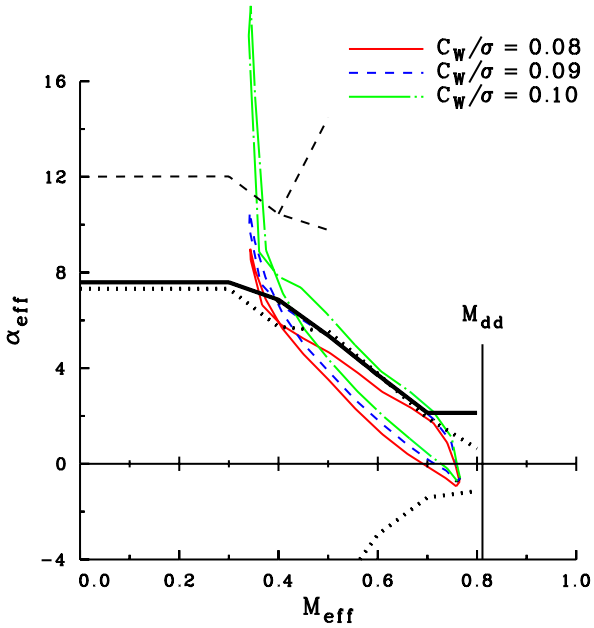

b. 0.865*R* (SC1095 airfoil section).

Figure 10. – Calculated α_{eff}–M_{eff} loops at 0.835*R* and 0.865*R* for three weight coefficients compared to basic airfoil characteristics.

on the blade. Calculations were made with the CAMRAD II analysis for linear twist values from –4 to –24 deg. Figure 11 shows the rotor *L/D* at $C_W/\sigma = 0.10$ for six values of blade twist. A twist of –16 deg represents the baseline condition. At this weight coefficient, the configurations with twist from –16 to –24

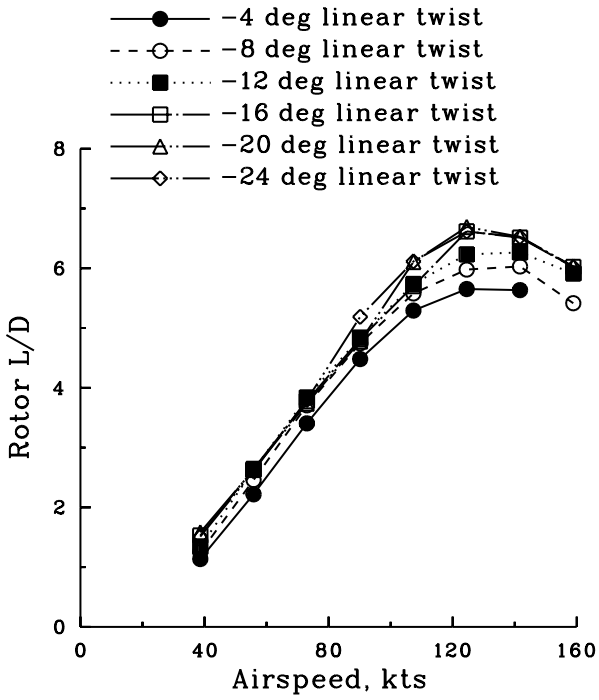

Figure 11. – Rotor *L/D* as a function of airspeed for six built in twist angles; $C_W/\sigma = 0.10$.

deg show comparable performance. The configurations with less twist, from –12 to –4 deg show progressively reduced performance. Fig. 12 shows the radial distribution of the azimuthal mean of the *L/D* deficiency angle as a means of characterizing the airfoil performance for these cases. This figure shows that the effect of twist is to even out the distribution of the deficiency angle from root to tip. For the highest twist value, the mean azimuthal value is roughly bounded between 0 and –2 deg from root to tip. At the lowest twist, –4 deg, the azimuthal mean ranges from –5 deg near the root to almost +2 deg on the outboard section.

Figure 13 shows α_{eff}–M_{eff} loops for twist values of –8, –16, and –24 deg at two radial stations for $\mu = 0.33$ and $C_W/\sigma = 0.10$. The loops are shown inboard at 0.44*R* and outboard at 0.865*R*, where the built-in twist was observed to have the greatest effect in Fig. 12. At 0.44*R* all of the twist cases show retreating blade stall, although this occurs for $M < 0.10$ and the loads are small. Around most of the rotor azimuth the deficiency angle is quite negative for the –8 deg twist case. The loop for the –24 deg case, however, exceeds the best *L/D* line for a significant range of azimuths and is also outside the drag bucket boundary, indicating reduced performance. Outboard, at 0.865*R*, the loop for the –24 deg twist case stays mostly within the upper boundary of the drag

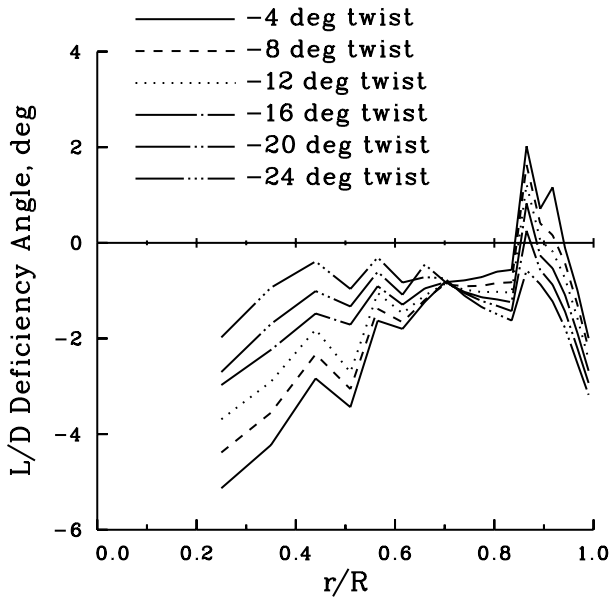

Figure 12. – Azimuthal mean of the *L/D* deficiency angle as a function of radial station for six values of built-in twist; $\mu = 0.33$, $C_W/\sigma = 0.10$.

bucket and stall doesn't occur as it does with the –16 deg twist case. Note, however, that on the advancing side, the airfoil is starting to penetrate the lower edge of the drag bucket for the –24 deg case and the associated drag penalty becomes progressively worse towards the tip of the blade. The loop for the –8 deg twist case at 0.865*R* shows more severe stall than the –16 deg case and is also outside of the drag bucket for a considerable range of azimuths, indicating an increased drag penalty.

Although the radial distribution of the mean azimuthal *L/D* deficiency angle in Fig. 12 suggests that a more highly twisted rotor is better in terms of airfoil *L/D*, a detailed examination of the α_{eff} –M_{eff} loops indicates that other factors, such as the drag rise at negative angles of attack near the blade tip for highly twisted rotors may be just as important.

Effects of Rotor Speed Variation

Increases in rotor speed offer the possibility of reducing blade stall, but at a cost of increased drag on the advancing side. Decreases in rotor speed have the opposite effect of decreasing the drag on the advancing side but increasing blade stall on the retreating side. The case of $C_W/\sigma = 0.10$ (GW = 21,075 lb) is a severe test of the effects of rotor speed variation, as the baseline calculations have shown that the performance is already degraded for this condition by blade stall outboard on the blade. The rotor *L/D* is shown as a function of forward

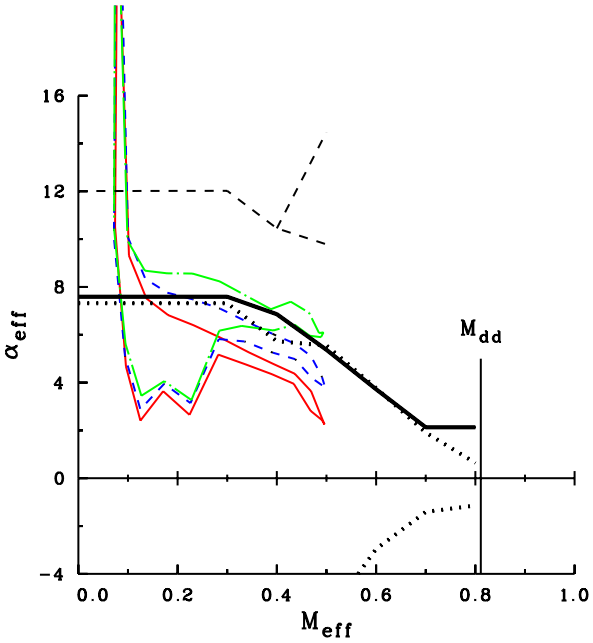

a. 0.44*R* (SC1095 airfoil section).

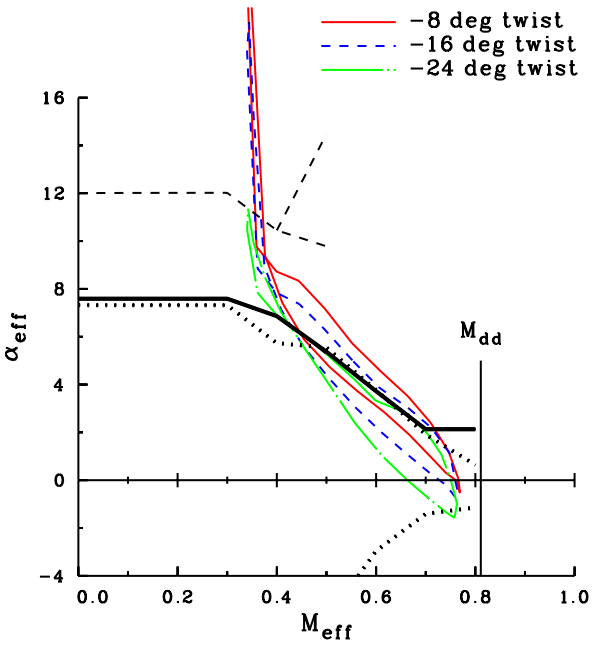

b. 0.865*R* (SC1095 airfoil section).

Figure 13. – Calculated α_{eff}–M_{eff} loops at 0.44*R* and 0.865*R* for three built-in twist values; $\mu = 0.33$, $C_W/\sigma = 0.10$.

speed in Fig. 14 for five values of rotor speed, from 92% to 108%. The weight and airspeed were held constant for these calculations, which means that the weight

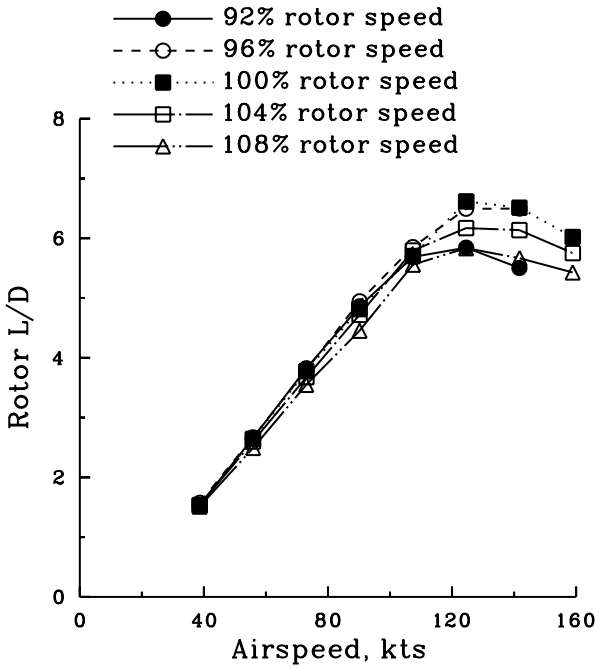

Figure 14. – Rotor *L/D* as a function of airspeed for six rotor speeds; *GW* = 21,075 lb.

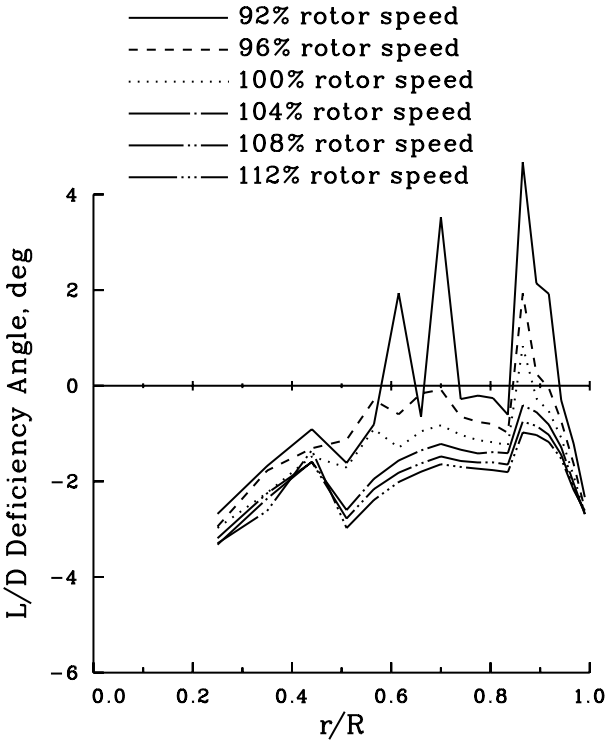

Figure 15. – Azimuthal mean of the *L/D* deficiency angle as a function of radial station for six rotor speeds; *V* = 142 kts, *GW* = 21,075 lb

coefficient and advance ratio will vary with the rotor speed. The best rotor *L/D* is obtained for rotor speeds of 96 and 100%. Decreased performance is observed for both higher and lower values of rotor speed.

The radial distribution of the azimuthal mean of the *L/D* deficiency angle is shown in Fig 15 for the case of *V* = 142 kts and *GW* = 21,075 lb. The 100% case is the same baseline case as shown previously and the deficiency angle is positive on the outer blade because of stall (see Fig. 10). Increases in the rotor speed have reduced the deficiency angle outboard, suggesting that the previously observed stall effects are ameliorated. It is anticipated, however, that these increased speeds will result in drag penalties on the advancing blade tip, but these penalties are not reflected in the *L/D* deficiency angle.

Figure 16 shows α_{eff} –M_{eff} loops at two outboard stations for this flight case for three values of rotor speed. The effect of the increased rotor speed is to reduce the stall on the outer blade and also to reduce the extent of the azimuth where the loops exceed the best *L/D* line and the drag bucket boundary. However, on the advancing side the loops extend to higher Mach numbers and, based on the rotor *L/D* comparison in Fig. 14, the increased drag penalty appears to degrade the global performance. In terms of rotor *L/D*, both the 96 and 100% cases show better performance despite the increased blade stall seen on the outer blade.

Design Criteria

Based on the calculations shown in this paper there is a correspondence between global performance measures, such as rotor *L/D*, and the airfoil section environment as relates to the angle of attack for maximum airfoil *L/D*, the boundary of the drag bucket, and the drag rise associated with the airfoil divergence Mach number. In particular, the definition of the *L/D* deficiency angle, which is a function of both azimuth and radius, provides a conceptual framework to understand why improvements of helicopter rotors and airfoils remain a difficult design problem. An optimal rotor design is one that can reduce the *L/D* deficiency angle over all r and ψ, while at the same time ensuring that other boundaries, such as the divergence Mach number and the stall boundary are not exceeded.

If one is to optimize a rotor over r and ψ, so that the *L/D* deficiency angle is close to zero, then it is necessary to do this through blade and airfoil design or with controls. The use of 2/rev or higher harmonic controls may provide some utility in the future. In this context, however, it is useful to distinguish between azimuthal

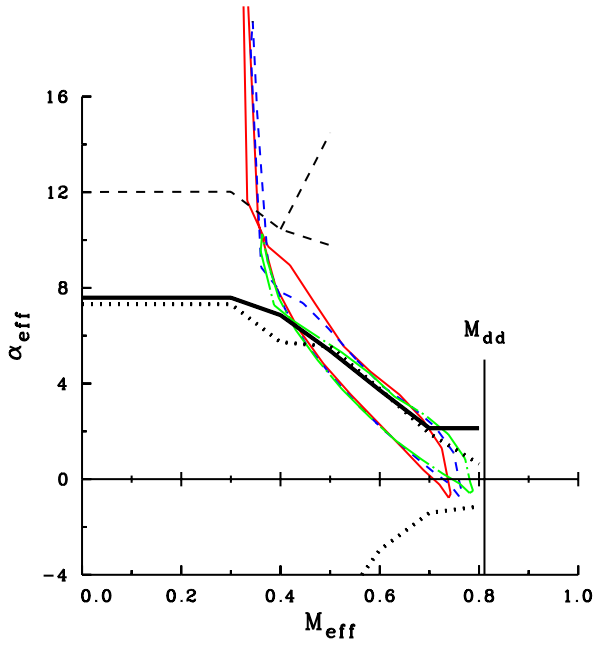

a. 0.865*R* (SC1095 airfoil section).

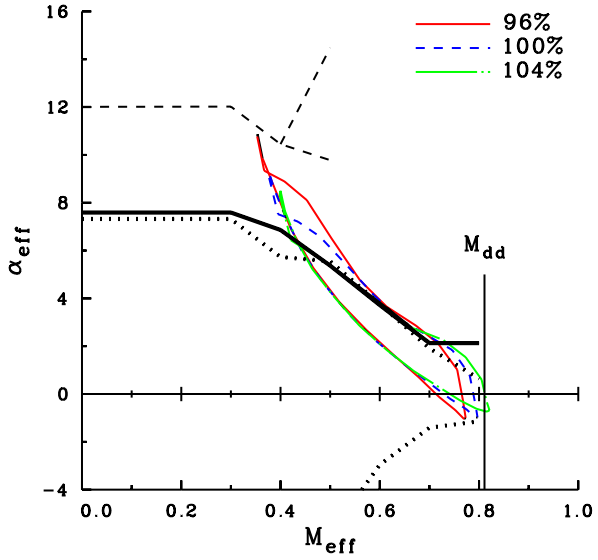

b. 0.9175*R* (SC1095 airfoil section).

Figure 16. – Calculated α_{eff}–M_{eff} loops at 0.865*R* and 0.9175*R* for three rotor speeds; V = 142 kts, GW = 21,075 lb.

controls, such as used in an individual blade control scheme and radial controls that might be implemented with multiple blade flaps.

The classical helicopter airfoil design approach is to develop high-speed airfoils that have a high divergence Mach number for use near the blade tip on the advancing side, and high-lift airfoils with a high $C_{l_{max}}$, for use on the retreating side. However, the use of an L/D deficiency angle, as discussed here, does not directly relate to the drag rise that is associated with divergence Mach number. This suggests that a criteria that puts more weighting on the drag boundaries might be more useful. For the retreating side of the rotor a criteria based on the L/D deficiency angle is more directly related to the use of $C_{l_{max}}$. As an example, Figure 17 shows this relation for seven helicopter sections tested in a single wind tunnel for M = 0.30 (Ref. 12). The fit between maximum L/D and $C_{l_{max}}$ is quite good for these tests (excluding the supercritical wing section that was also included in these tests). Data obtained at M = 0.40 in 31 separate airfoil tests are shown in Fig. 18 (Ref. 13). The relationship between the maximum L/D and $C_{l_{max}}$ in this case is not as good as in the previous figure. Particularly notable are some airfoils with excellent L/D's and poor $C_{l_{max}}$'s and other airfoils where the converse is true. This suggests, at the least, that new airfoil designs with high $C_{l_{max}}$ values should be tested to ensure that their maximum L/D values are also advanced.

Concluding Remarks

The CAMRAD II analysis has been used to examine the relations between global performance of a typical helicopter and the airfoil environment as represented by the airfoil angles of attack and Mach number. A general correspondence is observed between global performance parameters, such as rotor L/D, and airfoil performance parameters, such as airfoil L/D, the drag bucket boundaries, and the divergence Mach number. Whereas an airfoil for fixed-wing applications need only be optimized for a limited range of angles of attack and Mach number, the helicopter section airfoil needs to be optimized over all radial sections and azimuths, which is a difficult and complicated problem.

Effects of design parameters such as blade twist and rotor speed variation have been examined and, in most cases, improvements observed in global performance are also observed in terms of airfoil performance. However, it has been shown in a number of cases that changes that are obvious improvements in one region of the rotor disk have penalties in another part of the disk and these conflicts are difficult to resolve. Such results, of course, are not novel, and are familiar barriers to all rotor designers.

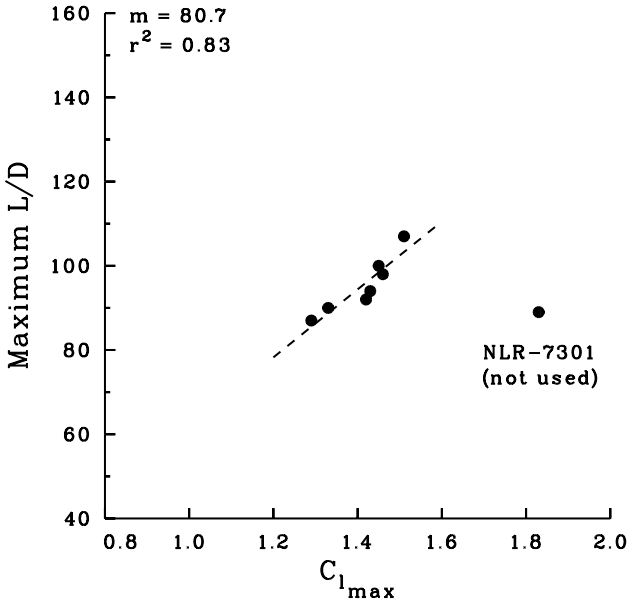

Figure 17. – Correlation of maximum *L/D* with maximum lift coefficient for seven helicopter airfoil sections (Ref. 12).

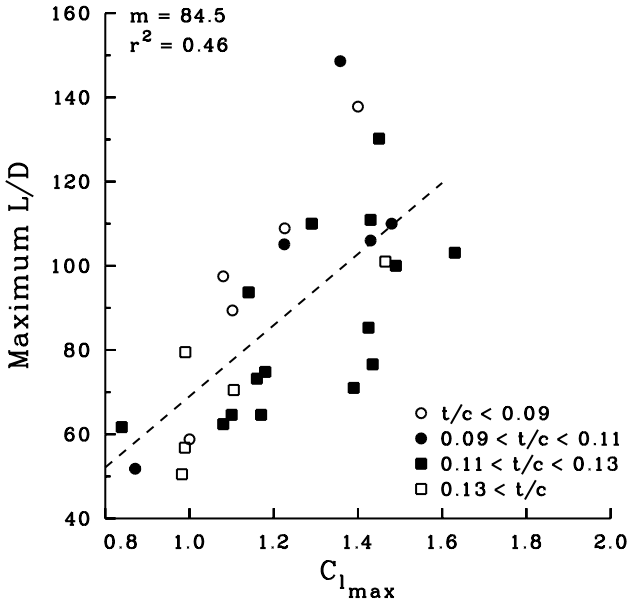

Figure 18. – Correlation of maximum *L/D* with maximum lift coefficient for 31 airfoil sections (Ref. 13).

The focus of this paper on airfoil section *L/D* instead of $C_{l_{max}}$ follows the observation that good airfoil and helicopter performance is best achieved under normal operating conditions when good airfoil *L/D* is obtained. This is not to suggest that good $C_{l_{max}}$ is not important, only that it should never be achieved at the expense of good *L/D*.

References

1. Bezard, H., "Rotor Blade Airfoil Design by Numerical Optimization and Unsteady Calculations," American Helicopter Society 48th Annual Forum Proceedings, Washington, D.C., June 3-5,1992, pp. 1283-1294.

2. Vozhdajev, E. S., and Golovkine, V. A., "Current State-of-the-Art of TsAGI Studies in the Area of Helicopter Aerodynamics," Twenty First European Rotorcraft Forum Proceedings, Saint Petersburg, Russia, August 30-September 1, 1995.

3. Kondo, N., Nishimura, H., Nakamura, H., Aoki, M., Tsujiuchi, T., Yamakawa, E., Aoyama, T., and Saito, S., "Preliminary Study of a Low Noise Rotor," Paper No. 22, Twenty-third European Rotorcraft Forum, Dresden, Germany, September 16-18, 1997.

4. Johnson, W. "CAMRAD II, Comprehensive Analytical Model of Rotorcraft Aerodynamics and Dynamics." Johnson Aeronautics, Palo Alto, California, 1992–1999.

5. Johnson, W. "Technology Drivers in the Development of CAMRAD II," American Helicopter Society, Aeromechanics Specialists Conference, San Francisco, January 19-21, 1994.

6. Noonan, K. W., and Bingham, G. J., "Aerodynamic Characteristics of Three Helicopter Sections at Reynolds Numbers from 0.35 to 0.9," NASA TM-86719, September 1980.

7. Yeo, H., Bousman, W. G., and Johnson, W., "Performance Analysis of a Utility Helicopter with Standard and Advanced Rotors," American Helicopter Society Aerodynamics, Acoustics, and Test and Evaluation Technical Specialist Meeting, San Francisco, CA, January 23-25, 2002.

8. Kufeld, R. M., Balough, D. L., Cross, J. L., Studebaker, K. F., Jennison, C. D., and Bousman, W. G., "Flight Testing the UH–60A Airloads Aircraft," American Helicopter Society 50th Annual Forum Proceedings, Washington, D.C., May 11-13, 1994, pp. 557–578.

9. Hooper, W. E., "The Vibratory Airloading of Helicopter Rotors," *Vertica*, Vol. 8, 1984, pp.

71–92. Also: Paper No. 46, Ninth European Rotorcraft Forum, Stresa, Italy, September 13-15, 1983.

10. Lim, J. W., "Analytical Investigation of UH–60A Flight Blade Airloads and Loads Data," American Helicopter Society 51st Annual Forum Proceedings, Ft. Worth, TX, May 9-11, 1995, pp. 1156–1175.

11. Bousman, W. G., "Putting the Aero Back Into Aeroelasticity," Eight ARO Workshop on Aeroelasticity of Rotorcraft Systems, University Park, PA, October 18-20, 1999.

12. McCroskey, W. J., McAlister, K. W., Carr, L. W., and Pucci, S. L., "An Experimental Study of Dynamic Stall on Advanced Airfoil Sections," NASA TM-84245, July 1982.

13. Dadone, L. U., "U.S. Army Helicopter DATCOM, Volume I – Airfoils," Boeing Doc. No. D210-11097-1, May 1976.